Propulsive Heading Control and Damping-Induced Heading Recovery for a Free Hydrofoil with an Internal Rotor

Scott David Kelly Rodrigo Abrajan-Guerrero

***Abstract*— Regulating the heading of a free planar hydrofoil by spinning a rotor mounted to the foil using linear feedback can generate forward propulsion as a byproduct, and sufficient variety exists among heading controllers of this kind to regulate the foil's translational speed in parallel without a second control input. Regulating the heading of the foil is complicated, however, by a recovery phenomenon resulting from viscous drag whereby reorientation of the foil during actuation is partly undone once actuation is ceased. Aspects of this phenomenon can be reproduced by a relatively simple nonlinear model.**

I. INTRODUCTION

This paper concerns the planar self-propulsion and maneuvering of a free rigid hydrofoil with a balanced internal rotor. The system is depicted schematically in the left panel of Fig. 1. A solitary control input regulates the difference in orientation between the foil and the rotor. Spinning the rotor relative to the foil induces the foil to counter-spin; lateral movement of the foil's trailing point through a surrounding fluid generates a propulsive force with a nonzero component aligned along the foil's axis of symmetry. This force reflects the shedding of vorticity from the foil's trailing point in accordance with variations in the circulatory flow around the foil. The foil's vortical wake advects momentum away from the foil and the foil attains contrary momentum in the balance. The rotor is "internal" in the sense that it doesn't interact directly with the surrounding fluid. A physical realization of this system is depicted in the right panel of Fig. 1. The foil takes the form of a styrofoam raft two and a half centimeters thick that floats with roughly half this thickness submerged when placed in water. The rotor is mounted atop the raft to isolate it from the water.

A system analogous to that in Fig. 1, comprising a rotor mounted not atop a raft in a fluid but atop a platform supported — like a typical shopping cart is supported — by casters in front and by wheels in the rear, was introduced in [1] and named the *Chaplygin beanie*.[1] The present system and the Chaplygin beanie share the feature that lateral movement is resisted in the rear but not in the front, as a consequence of which a rotor-driven oscillation in heading will necessarily give rise to forward propulsion. It was shown in [1] that if the Chaplygin beanie is initially at rest, then it's possible to vary the relative heading of the rotor thereafter in a manner that will drive the system to translate asymptotically at an arbitrary heading with an arbitrary translational speed. In particular, a proportional controller of the form $\ddot{\phi} = k\theta$ (in the notation of Fig. 1) was shown analytically to drive the heading angle θ asymptotically to zero as the system approached a steady translational speed depending monotonically on the constant feedback gain k.

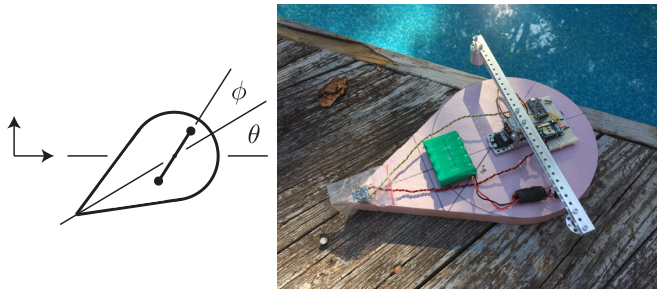

Fig. 1. A planar aquatic vehicle comprising a rigid hydrofoil coupled to a balanced rotor. Spinning the rotor counter-rotates the foil; oscillations in the foil's heading generate forward propulsion. The styrofoam foil on the right is thirty-six centimeters long and twenty-four centimeters wide.

The system in Fig. 1 is susceptible to primitive control of this kind only to a limited degree, primarily because the resistance to lateral motion at the rear of the foil is not absolute as it is in the case of a nonholonomically constrained cart with wheels. The force that resists lateral motion at the rear of the foil isn't a force of constraint, but is instead a force that dissipates energy as the foil rotates. This dissipation of energy exposes the system to the phenomenon termed *damping-induced self-recovery* in [6], [7], [8], whereby the rotor-driven rotation of a body subject to (exclusively or partly) viscous drag will be (entirely or partly, respectively) undone when rotor motion stops. A mathematical analysis of self-recovery in the presence of purely viscous drag appears in the preceding references.

In section II, we demonstrate with laboratory data that the essential premise of [1] — that regulation of the Chaplygin beanie's heading will engender forward propulsion as a byproduct, and that sufficient freedom is available in the design of heading controllers to accommodate the additional regulation of translational speed — also applies to the system in Fig. 1. In section III, we demonstrate that if the dissipative moment resisting rotation of the foil is linear in $\dot{\theta}$, then the self-recovery phenomenon prohibits permanent reorientation of the foil as a result of finite-time changes in the relative orientation of the rotor, but that nonlinearity in this moment

Rodrigo Abrajan-Guerrero and Scott David Kelly are with the Department of Mechanical Engineering and Engineering Science, University of North Carolina at Charlotte, Charlotte, NC 28223, USA.

This material is based upon work supported by the National Science Foundation under grants CMMI-1000652.

Correspondence should be directed to `scott@kellyfish.net`.

[1]The Chaplygin beanie combines features of two canonical systems from the mechanics literature, *Elroy's beanie* ([2], [3]) and the *Chaplygin* (or *Carathéodory*) *sleigh* ([4], [5]).

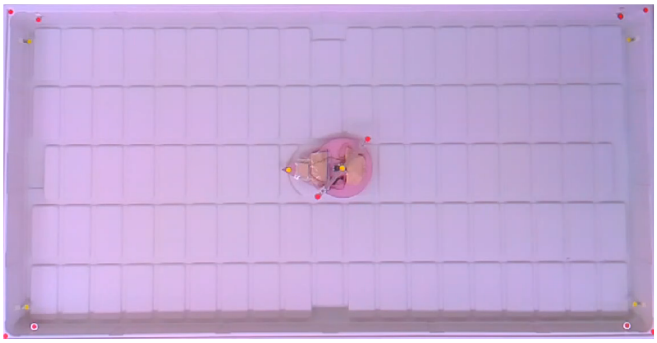

Fig. 2. The laboratory pool with the foil in the center as viewed from a camera mounted three meters above. The red tone in the image is the result of brightness, saturation, and white balance settings that were determined to facilitate tracking of the colored markers. The pool floor is actually white.

may be exploited to attenuate recovery. In section IV, we draw attention to a saturation phenomenon that sometimes accompanies damping-induced recovery, presenting a model-based analysis to guide future physical experiments.

II. PROPULSION THROUGH HEADING CONTROL

Proportional and integral feedback control laws were tested for regulating the heading of the physical foil shown in Fig. 1. The measurement of θ was obtained using the STMicro L3DG20H gyrometer contained within a ten-degree-of-freedom inertial measurement unit available from Adafruit. The gyrometer measures angular velocity, which can be integrated to obtain angular position over short periods of time. Only the z-axis measurement was used; the sensor was mounted on the tail of the foil with this axis pointed upward. The control routine was programmed to an Adafruit Pro Trinket, an ATMega328-based microcontroller. An XBee radio module was used to enable serial communication between the microcontroller and a PC so that control parameters could be adjusted remotely during testing. The rotor visible in Fig. 1 comprises a length of aluminum Actobotics "mini channel", to which weights can be affixed at a variety of locations to vary the rotor's inertia, mounted atop a Hitec HSR-1425CR continuous-rotation servomotor. Also visible in the figure is a 6V 2200mAh NiMH battery used to power the servo, microcontroller, XBee, and sensors.

Experiments were performed in a 240×120 centimeter pool, shown in Fig. 2, filled with water roughly eight centimeters deep. A Raspberry Pi with a camera module was mounted three meters above the pool to record video, from which trajectories of the foil's extremes and the rotor's extremes could be extracted. The camera was used only to collect data for post-processing; the microcontroller used only measurements from the IMU to regulate the behavior of the rotor. A projective transformation was used to convert trajectories in the camera's view to real-world coordinates. The stationary markers visible in the corners of the pool in Fig. 2, situated at different heights to match the heights of the markers on the foil and rotor, facilitated realization of this transformation.

Each experiment began with the foil at rest near one end of the pool, where it would receive a command to reorient counterclockwise to increase the heading angle θ from zero to $\pi/18$ radians using a PI controller to determine the angular velocity of the servo from the foil's orientation. Fig. 3 shows the trajectories obtained with five different sets of control gains, three corresponding to purely integral control (on the left) and two corresponding to purely proportional control (on the right). The trajectory of the center of the rotor is shown in each case for a period of twenty-six seconds, corresponding to the time required for the integral controller with $k_i = 7$ to bring the foil in contact with the opposite end of the pool. Both panels show that different gains yield different swimming speeds. Gradual drift is apparent in the foil's heading, particularly in the case of purely integral control; the authors expect this drift to disappear from future experiments when camera data rather than gyrometer measurements are used to inform the microcontroller of the foil's heading.

Fig. 4 depicts heading data corresponding to the trajectory data of Fig. 3. It's apparent that purely integral control engenders forward propulsion more reminiscent of the swimming of fish, whereby the nose of the foil repeatedly overshoots its average heading to a substantial degree as the foil moves forward. Purely proportional control (with the chosen gains) engenders higher-frequency vibrations in heading that contribute to the observed drift in gyrometer measurements.

III. DAMPING-INDUCED HEADING RECOVERY

A. Modeling

For the remainder of the paper, we concern ourselves with the dynamics and control of the foil's heading alone, and not with the propulsion that results from varying this heading. It might seem that the most straightforward way to reorient the foil permanently — say, clockwise, decreasing θ from zero to a negative constant over a certain period of time — would be to spin the rotor in the opposite direction until the desired reorientation had been achieved, and then to discontinue actuation. A fundamental obstacle to this strategy is present in the mechanics of the system, however, that results from the viscous drag exerted on the foil by the water. This can be illustrated concretely as follows.

Fig. 5 depicts a smooth bump function of the form

$$b(w,t) = \begin{cases} \exp\left(\frac{a^2}{a^2-1}\right) & 0 < t < w \\ 0 & \text{otherwise} \end{cases} \quad (1)$$

where

$$a = \frac{2t}{w} - 1.$$

If $\dot{\phi}$ is set equal to $b(w,t)$, the rotor will accelerate smoothly from rest to a maximum angular velocity of 1 rad / s counterclockwise and then decelerate symmetrically, coming to rest (relative to the foil) at $t = w$. For every simulation described in this section of the paper, $\dot{\phi}$ corresponds to a linear combination of such functions.

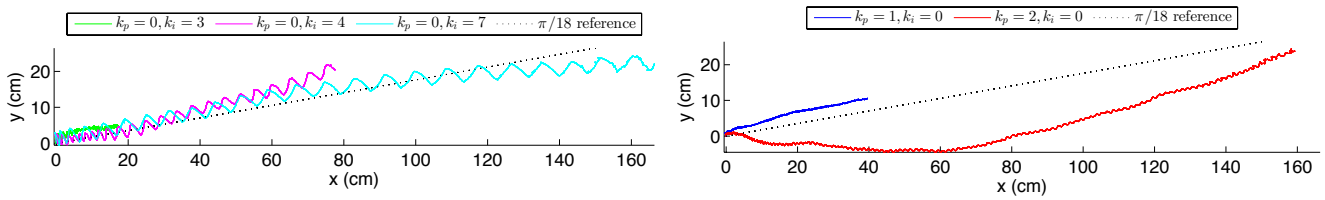

Fig. 3. Swimming trajectories obtained as byproducts of heading control using purely integral (left) or purely proportional (right) feedback.

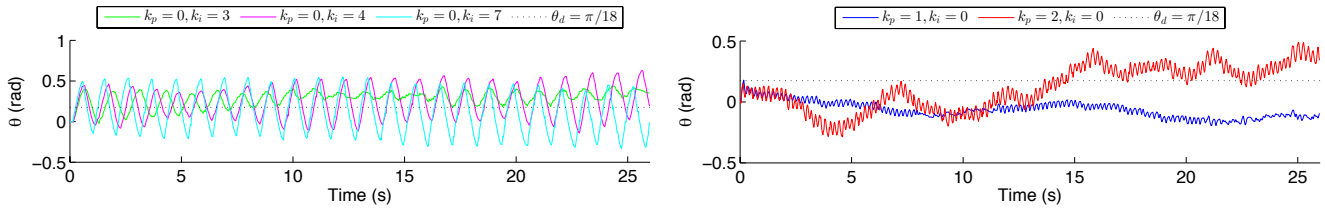

Fig. 4. Heading data corresponding to the trajectories shown in Fig. 3.

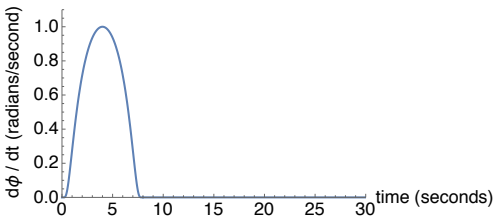

Fig. 5. Relative counterclockwise rotor speed corresponding to the three simulations represented in Fig. 6, given by (1) with w equal to eight seconds.

In the absence of dissipation, the rotational dynamics of the foil and rotor together are governed by the conservation of total angular momentum. If F and B denote the effective rotational inertias of the foil and rotor, respectively, then this conservation law is equivalent to the differential equation

$$F\ddot{\theta} + B(\ddot{\theta} + \ddot{\phi}) = 0.$$

The form of this equation is unchanged by the fact that the effective inertia of the foil may include added inertia inherited from the surrounding fluid. The top panel in Fig. 6 depicts the variations in θ and ϕ that occur over time when $\theta = \dot{\theta} = \phi = 0$ initially, $\dot{\phi}$ is given by the bump function shown in Fig. 5, F and B are assigned the (arbitrary) values

$$F = 1 \text{ kg m}^2, \quad B = 5 \text{ kg m}^2,$$

and dissipation is absent from the system. Not surprisingly, spinning the rotor counterclockwise relative to the foil induces the foil to rotate clockwise, and the foil ceases to rotate when actuation is discontinued.

The introduction of damping to the system in the form of dissipative resistance to the foil's rotation doesn't merely attenuate the extent to which spinning the rotor will counter-rotate the foil. The hydrodynamic forces acting on a real rotating hydrofoil are complicated, and have high-order dynamics associated with vortex shedding and wake-body interactions (modeled computationally in [9]), but a primitive model can be obtained by focusing on the components of rotational drag that are linear or quadratic in rotational speed. In the presence of these, the conservation of angular momentum is superseded by the evolution equation

$$F\ddot{\theta} + B(\ddot{\theta} + \ddot{\phi}) = -\mu\dot{\theta} - \nu\dot{\theta}^2, \tag{2}$$

where μ and ν are positive constants.

The "self-recovery" phenomenon documented in [6], [7], [8] arises in the present context when μ is nonzero. The middle panel in Fig. 6 depicts the response in the foil's orientation to the same rotor motion depicted in the preceding panel when $\nu = 0$ but $\mu = 2$ kg m^2 / s. Initially, the foil counter-rotates in response to the spinning of the rotor, but once the rotor is brought to rest relative to the foil, the foil's heading returns all the way to its initial value. This behavior isn't specific to our choice of rotor motion: it's straightforward to show (using the final value theorem) that following any sequence of actuation that's bounded in time, θ will return asymptotically to its initial value. The asymptotic value of θ can't be altered through any finite-time sequence of actuation when drag linear in $\dot{\theta}$ — viscous drag — is present but additional nonlinear drag is not.

When both viscous drag and nonlinear drag act on the foil, heading recovery occurs only partly, but can still be substantial. We demonstrate this experimentally in section III-B[2], but the inclusion of quadratic drag in (2) is sufficient to engender the phenomenon of partial recovery. The bottom panel in Fig. 6 depicts the response in the foil's orientation to the same rotor motion depicted in the preceding panels when $\mu = 2$ kg m^2 / s and $\nu = 1$ kg m^2. The angle θ reaches a minimum of -2.04 radians and then recovers to -0.597 radians.

Damping-induced heading recovery can represent a substantial obstacle to simple motion control for an aquatic vehicle, and one objective of the present paper is to identify a strategy for attenuating its influence. Such a strategy is

[2]A physical demonstration by the authors that predates the present paper is also visible at `http://tinyurl.com/ojoojj8`.

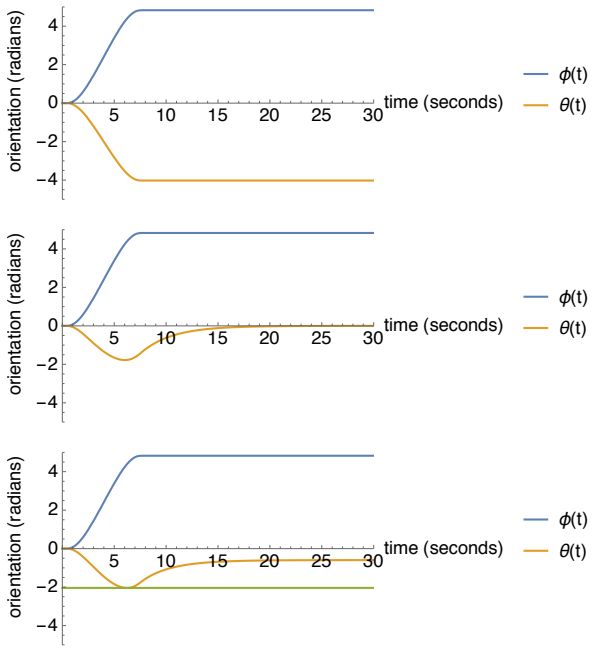

Fig. 6. Rotor orientation and foil orientation over time when the rotor's relative counterclockwise speed is as shown in Fig. 5 and damping is absent (top), exclusively linear in the foil's rotational speed (middle), or partly linear and partly quadratic in the foil's rotational speed (bottom).

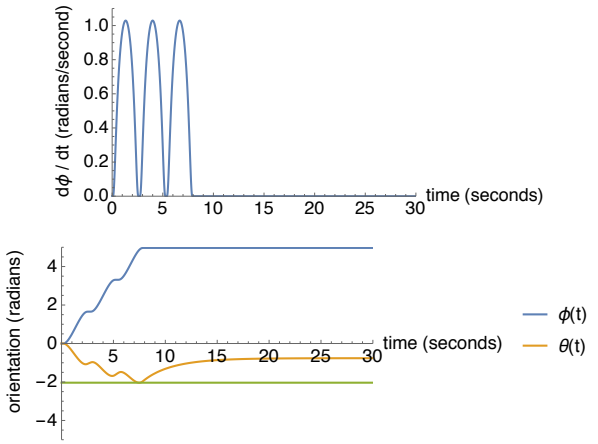

Fig. 7. Relative counterclockwise rotor speed (top) and rotor and foil orientation (bottom) demonstrating a 12% decrease in heading recovery compared to the bottom panel in Fig. 6 under the same parametric conditions. The minimum value of θ is -2.04 radians in both cases, indicated with a green line for visual comparison.

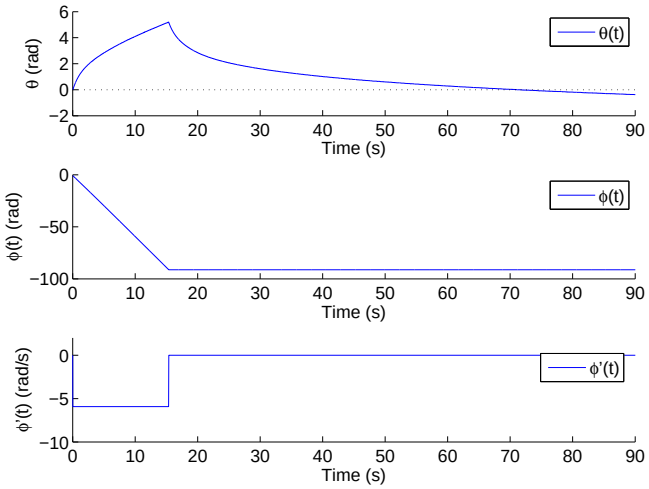

Fig. 8. Foil heading (top) as a function of time, exhibiting recovery after the rotor is spun for fifteen seconds at a constant speed relative to the foil and then stopped. The rotor's relative orientation (middle) and relative counterclockwise speed (bottom) are also shown.

suggested by Fig. 7, which depicts the outcome when — in the presence of both viscous and quadratic damping, parametrized as before — the rotor is spun up and down thrice rather than once in the same window of time, to a degree selected so that the foil is reoriented to the same extreme ($\theta = -2.04$ radians) before actuation is ceased. Subsequent recovery of the foil's heading (now to $\theta = -0.763$ radians) is diminished by more than ten percent. We infer that when nonlinear drag is present, damping-induced heading recovery may be curtailed by actuating the rotor to reorient the foil in a stepwise, rather than monotonic, fashion. We stress that this isn't true when drag is absent from the system (in which case no recovery occurs) or when only viscous drag is present (in which case complete recovery occurs) — both cases that can be treated analytically for arbitrary rotor motions.

B. Experiments

Using the same test setup as for the experiments in section II, the system was programmed to rotate the rotor at a constant speed for a specific amount of time and then to terminate actuation. The heading angle θ was measured during the rotor's motion and thereafter to document damping-induced recovery.

Fig. 8 depicts the outcome of one such experiment. The angular velocity of the rotor was set to -5.9 rad/s for fifteen seconds and then to zero for seventy-five seconds more; the foil's heading increased while the rotor was spinning and then returned to its initial value thereafter. The data actually show an overshoot in the foil's heading after recovery, but this was apparently due to persistent excitation of the water (confined by nearby rigid boundaries) following the foil's initial motion. Fig. 9 shows the trajectories followed by markers at the center of the rotor and the tail of the foil during this experiment. These two points are used to obtain the foil's heading. The green and red arrows indicate the initial and final positions of the foil, respectively; each arrow points from the foil's tail to the center of the rotor.

Figs. 10 and 11 depict the outcome of a second experiment in which the rotor was spun for forty seconds and then stopped. Heading recovery is clearly partial in this case; the angle θ increased from zero to 11.4 radians during actuation and then recovered 43% to 6.5 radians thereafter.

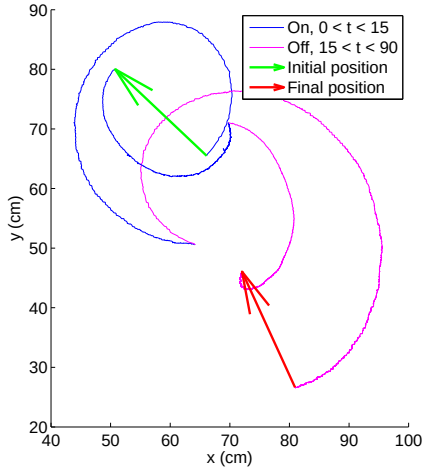

Fig. 9. Trajectories of the center of the rotor and the rear of the foil corresponding to the data in Fig. 8.

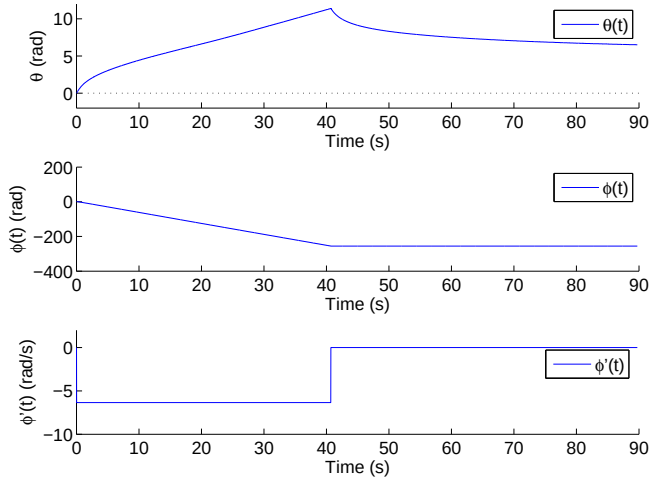

Fig. 10. Foil heading (top) as a function of time, exhibiting partial recovery after the rotor is spun for forty seconds at a constant speed relative to the foil and then stopped. The rotor's relative orientation (middle) and relative counterclockwise speed (bottom) are also shown.

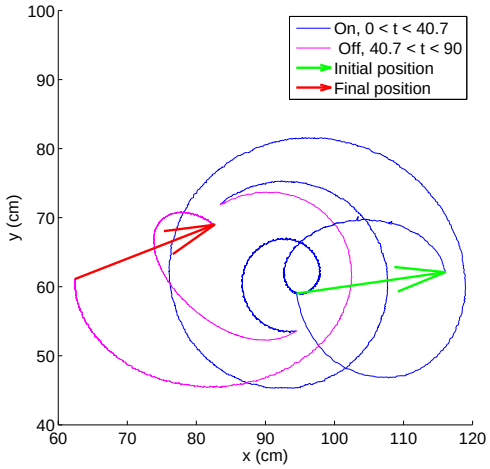

Fig. 11. Trajectories of the center of the rotor and the rear of the foil corresponding to the data in Fig. 10

IV. DISCUSSION

The system considered in this paper is worthy of study partly because of its simplicity. Problems concerning the coupling of steering to propulsion or the influence of damping on heading control are common to many aquatic vehicles; the present system isolates these in a uniquely elemental setting. Because the system isn't merely underactuated but *singly* actuated, its dynamics include no component attributable to *geometric phase*, which plays a substantial role in certain forms of aquatic locomotion [10]. The present paper considers for the first time the notion of partial heading recovery in the presence of a mixture of linear and nonlinear damping. Our treatment of control in the presence of this phenomenon has been preliminary; we conclude by highlighting an additional relevant feature of systems with nonlinear damping that will be addressed in detail in a followup paper.

The movie linked in the footnote on page three illustrates a mechanical corollary to the principle of damping-induced recovery. When the rotor atop the foil in the movie is spun at a constant speed for a relatively long time in one direction, the foil doesn't counter-rotate at a constant speed, but instead counter-rotates with decreasing speed, approaching a state in which the foil's orientation is constant despite ongoing actuation. This behavior was *not* exhibited by the physical system depicted in Fig. 1 in the course of performing experiments for this paper. The two systems are essentially the same in design but differ in size and mass. The authors have yet to document the conditions under which this sort of saturation does or doesn't occur in the laboratory, but the simplified model (2) suggests the roles played by inertia and damping.

Suppose that the modeled system from Section III-A is initially at rest with F, B and μ assigned the values represented in the lower two panels in Fig. 6 and in Fig. 7. Now suppose that the rotor is driven so that $\dot{\phi}$ is a step function with magnitude k. Fig. 12 depicts the outcome when $k = 1$ rad / s and ν assumes four different values (measured in kg m^2).

In the absence of nonlinear damping, the system exhibits the saturation phenomenon described above and θ approaches -2.50 radians asymptotically over time. The introduction of nonlinear damping doesn't initially disrupt the system's tendency to saturate, but increases the discrepancy between the initial and asymptotic values of θ. If ν is increased beyond a critical value, however, persistent spinning of the rotor enables persistent counter-rotation of the foil.

Fig. 13 clarifies the transformation that occurs with a trio of phase portraits. The premise that the system is at rest before the rotor begins to spin requires that $\dot{\theta} = -kB/(F + B)$ initially (when the step input becomes nonzero). The system's initial condition is indicated with a black dot in each phase portrait; saturation occurs if the trajectory passing through this point approaches the horizontal axis in forward time.

The top panel in Fig. 13 corresponds to the case in which $\nu = 0$. The vector field with components $(\dot{\theta}, \ddot{\theta})$ has constant

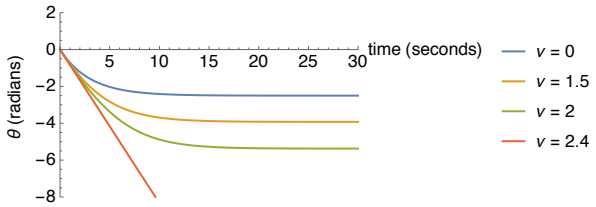

Fig. 12. Saturation in the foil's heading in response to constant spinning of the rotor with $\dot{\phi} = 1$ rad / s for positive time. The system is assumed to have been at rest prior to actuation. The parameters F, B, and μ assume the same values as in the lower two panels of Fig. 6 and in Fig. 7. Each curve corresponds to a different degree of quadratic damping in the system; ν is measured in kg m^2.

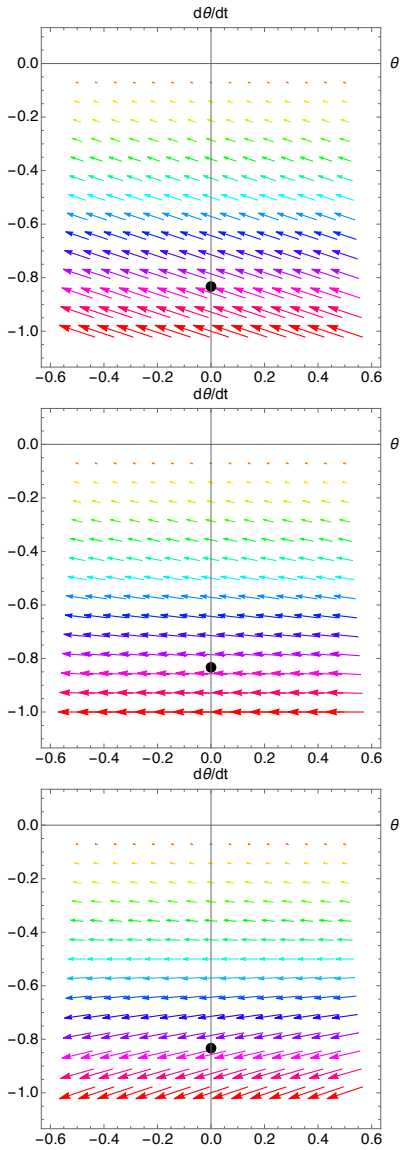

Fig. 13. Phase portraits derived from (2) that clarify whether or not the system with zero angular momentum prior to actuation will approach the saturated state $\dot{\theta} = 0$ once the rotor is spun counterclockwise with constant unit speed. In all three cases, F, B, and μ assume the same values as in the lower two panels of Fig. 6 and in Fig. 7. The top, middle, and bottom panels correspond to $\nu = 0$, 2, and 4 kg m^2, respectively.

slope throughout the phase plane — vectors in the upper half plane (not shown) are anti-parallel to vectors in the lower half-plane — and saturation occurs from every initial condition. The middle panel corresponds to the case in which $\nu = 2$ kg m^2. All the initial conditions shown in the lower half-plane lead to saturation, but the upward component of the phase flow diminishes with distance from the horizontal axis. The bottom panel corresponds to the case in which $\nu = 4$ kg m^2. The vertical component of the phase flow reverses sign along the horizontal line $\dot{\theta} = -\mu/\nu = -0.5$ rad / s, and saturation occurs when the system begins at rest (prior to actuation) because the initial condition indicated with a black dot lies below this line. The criterion for saturation with this initial condition is

$$kB\nu < (F + B)\mu.$$

Note that heading saturation of this kind need not be considered a liability. It can always be overcome with a more sophisticated choice of control, and it can be exploited to advantage when the control objective is to approach a certain heading without overshoot. The authors intend to explore this idea in the immediate future.

References

[1] S. D. Kelly, M. J. Fairchild, P. M. Hassing, and P. Tallapragada. Proportional heading control for planar navigation: The Chaplygin beanie and fishlike robotic swimming. In *Proceedings of the American Control Conference*, pages 4885–4890, 2012.

[2] J. E. Marsden, R. Montgomery, and T. S. Ratiu. Reduction, symmetry, and phases in mechanics. *Memoirs of the American Mathematical Society*, 436, 1990.

[3] J. E. Marsden. *Lectures on Mechanics*. Cambridge University Press, 1992.

[4] A. M. Bloch. *Nonholonomic Mechanics and Control*. Springer Verlag, 2003.

[5] Richard Cushman, Hans Duistermaat, and Jedrzej Śniatycki. *Geometry of Nonholonomically Constrained Systems*. World Scientific, 2009.

[6] D. E. Chang and S. Jeon. Damping-induced self-recovery phenomenon in mechanical systems with an unactuated cyclic variable. *ASME Journal of Dynamic Systems, Measurement, and Control*, 135(2):021011, 2013.

[7] D. E. Chang and S. Jeon. On the damping-induced self-recovery phenomenon in mechanical systems with several unactuated cyclic variables. *Journal of Nonlinear Science*, 23:1023–1038, 2013.

[8] D. E. Chang and S. Jeon. On the self-recovery phenomenon for a cylindrical rigid body rotating in an incompressible viscous fluid. *ASME Journal of Dynamic Systems, Measurement, and Control*, 137(2):021005, 2015.

[9] S. D. Kelly and P. Tallapragada. Self-propulsion of free solid bodies with internal rotors via localized singular vortex shedding in planar ideal fluids. *European Physical Journal Special Topics*, 224(17):3185–3197, 2015.

[10] S. D. Kelly, P. Pujari, and H. Xiong. Geometric mechanics, dynamics, and control of fishlike swimming in a planar ideal fluid. In S. Childress, A. Hosoi, W. W. Schultz, and Z. J. Wang, editors, *Natural Locomotion in Fluids and on Surfaces: Swimming, Flying, and Sliding*. Springer, 2012.